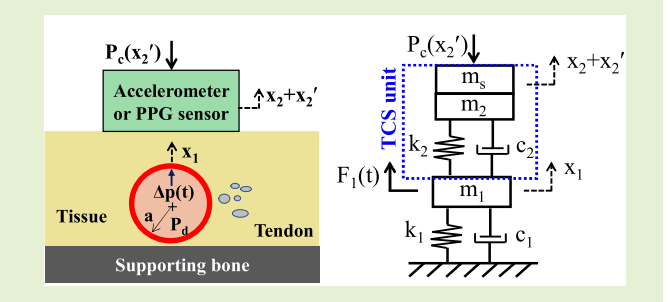


A 2-DOF Model of the Artery-Sensor System for Interpreting Variability in Measured Arterial Pulse Waveform

Zhili Hao

Abstract—This study presents a two degree-of-freedom (2-DOF) model of the artery-sensor system that accounts for contact pressure, sensor type, and overlying tissue above the artery in measured arterial pulse waveform (APW). While the arterial wall is treated as a one degree-of-freedom (1-DOF) unit, the tissue-contact-sensor (TCS) unit, formed by overlying tissue, sensor, and contact interface, is treated as another 1-DOF unit. Measured APW from three types of sensors: a photoplethysmography (PPG) sensor, an accelerometer, and a tactile sensor, is theoretically related to dynamic parameters of the TCS unit. With pulsatile pressure at the radial artery (RA) as the true APW, the measured APW is calculated



with different values of the dynamic parameters of the TCS unit. Due to its non-negligible damping and inertial terms, the TCS unit serves as a harmonics-dependent transfer function from the true APW to the measured APW. By determining dynamic parameters of the TCS unit, contact pressure, sensor type, and overlying tissue affect measured APW, and consequently the foot, peak, and other key features of measured APW. The natural frequency of the TCS unit plays a dominant role in affecting measured APW, as compared to its damping and spring stiffness. The myth of the influence of transmural pressure on arterial wall elasticity stems from negative pulsatile forces from the TCS unit. Motion artifacts introduce not merely additive noise (or baseline drift) but also multiplicative noise to measured APW, and thus minimizing motion artifacts is crucial for improving accuracy in measured APW.

Index Terms—Arterial indices, contact pressure, dynamic parameters, measured arterial pulse waveform (APW), motion artifacts, overlying tissue, pulsatile pressure, sensor type.

I. INTRODUCTION

RTERIAL pulse waveform (APW) carries more diagnostic values for the detection of cardiovascular (CV) disease, compared with arterial pulse amplitude [1], [2], [3]. APW has been utilized for estimating various arterial indices. In conjunction with an electrocardiogram (ECG) signal, both the foot and peak of APW at the periphery are utilized for estimating pulse transit time (PTT) [3], which can be further correlated to blood pressure for continuous cuffless blood pressure monitoring [3], [4]. While the first-order time derivative of APW is utilized to approximate blood velocity waveform, the ratio of minimum versus maximum of the second-order time derivative of APW is commonly used as an index for arterial stiffness [1], [5]. Features of APW and

Manuscript received 15 August 2023; accepted 21 August 2023. Date of publication 28 August 2023; date of current version 2 October 2023. This work was supported in part by the National Science Foundation, CBET Division, under Grant 1936005. The associate editor coordinating the review of this article and approving it for publication was Prof. Shakeb A. Khan.

The author is with the Department of Mechanical and Aerospace Engineering, Old Dominion University, Norfolk, VA 23539 USA (e-mail: zlhao@odu.edu).

Digital Object Identifier 10.1109/JSEN.2023.3307877

its two-time derivatives are also combined to estimate multiple arterial indices simultaneously [2]. As such, any variation in APW may affect the values of arterial indices derived from it.

Various sensors have been utilized to measure arterial pulse signals at the skin surface. Generally speaking, these sensors can be categorized into three types: accelerometers [6], [7], photoplethysmography (PPG) sensors [1], [3], [4], and tactile sensors [2], [8]. Contact pressure at the interface between a sensor and overlying tissue above the artery is needed so that the pulse signal in the artery can pass through the contact interface and transmit into the sensor [9]. Regardless of the type of sensor, it has been found that measured arterial pulse amplitude goes up as contact pressure increases, but goes down as contact pressure continues to increase. Contact pressure corresponding to the maximum measured pulse amplitude is commonly referred to as medium (or optimal) contact pressure [10]. Treated being the most accurate and with low noise, the measured APW with maximum amplitude is used for the estimation of arterial indices. Meanwhile, measured APW is also found to vary with contact pressure, and variation in measured APW leads to variation in estimated values of arterial indices [10], [11], [12], [13], [14]. Other than contact pressure,

1558-1748 © 2023 IEEE. Personal use is permitted, but republication/redistribution requires IEEE permission. See https://www.ieee.org/publications/rights/index.html for more information.

measured APW is found to noticeably vary with the sensor type [10] and sensor design [9]. Since calibration of measured arterial pulse amplitude varies with subject-specificity (i.e., overlying tissue above the artery) [1], [9], [15], [16], it is reasonable to infer that overlying tissue is another factor causing variation in measured APW.

Despite numerous experimental observations on the effect of contact pressure on measured APW, only two theoretical models have been proposed for interpreting the effect of contact pressure on PTT, based on experimental results using PPG sensors. Teng and Zhang [11] proposed a nonlinear biomechanical model of the arterial wall, where an exponential pressure-volume curve is used to explain the increase in PTT with contact pressure when transmural pressure P_T is positive, and constant PTT after P_T becomes negative. Chandrasekhar et al. [3] proposed a viscoelastic model of the arterial wall in the positive P_T territory, and a nonlinear model of the arterial wall in the negative P_T territory to explain a U-shaped trend of PTT with contact pressure. In both models, it is assumed that pulsatile pressure in the artery represents the true APW in an artery and remains unchanged by contact pressure, but arterial wall displacement, as the output of a PPG sensor, is affected by contact pressure, given that contact pressure affects P_T , with the latter affecting arterial wall viscoelasticity. However, these two models only considered the arterial wall and focused solely on the influence of contact pressure on measured APW, and the type of sensor and overlying tissue above the artery were excluded in the models.

Previously, the author's group developed a dynamic system model for the influence of contact pressure on measured arterial pulse amplitude and waveform when a tactile sensor is used for pulse measurement [15]. Although overlying tissue and sensor were included in this model, a detailed analysis of the influence of overlying tissue, sensor, and motion artifacts on measured APW was omitted. In this study, overlying tissue, a sensor, and their contact interface are combined into a tissue-contact-sensor (TCS) unit as a one degree-of-freedom (1-DOF) unit, and together with a 1-DOF model of the arterial wall, a two degree-of-freedom (2-DOF) model of the artery-sensor system is developed that accounts for the three factors: contact pressure, overlying tissue, and sensor type, involved in pulse measurement. This 2-DOF model is utilized to examine the role of dynamic parameters of the TCS unit in determining measured APW, investigate how motion artifacts are manifested in measured APW, and reveal the myth of the influence of transmural pressure on arterial wall elasticity.

II. METHODS

To analyze the artery-sensor system with different sensor types, three assumptions are made: 1) pulsatile pressure in the artery is treated as the true APW, and remains unchanged until the measured pulse signal passes its maximum amplitude; 2) transduction in a sensor is not considered, and then the related displacement in the 2-DOF model is used to represent the sensor output; and 3) the values of dynamic parameters of the TCS unit for different harmonics of the heart rate are the same and remain unchanged in a pulse cycle.

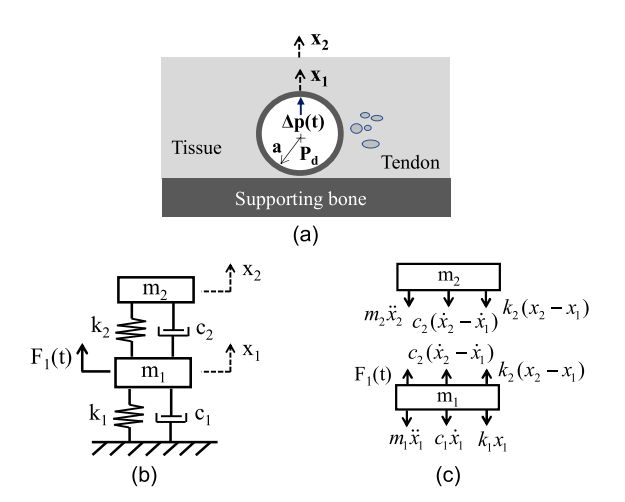


Fig. 1. Schematics of (a) artery embedded in its overlying tissue, (b) its equivalent 2-DOF model, and (c) force analysis on mass m_1 of the arterial wall and mass m_2 of the overlying tissue.

A. Artery and Its Overlying Tissue

As shown in Fig. 1(a), pulsatile pressure $\Delta p(t)$ in an artery causes arterial wall displacement $x_1(t)$. The force balance equation in its circumferential direction for the arterial wall is as follows [2]:

$$\rho \pi h a \frac{d^2 x_1}{dt^2} + \frac{h}{a} \pi \eta \cdot \frac{dx_1}{dt} + \frac{h}{a} \pi E \cdot x_1 = a \pi \Delta p \tag{1}$$

where E, η , and ρ are elasticity, viscosity, and density of the arterial wall, respectively; and h and a are the thickness and inner radius of the arterial wall, respectively. Only half of the arterial wall directly interacts with a sensor and is considered here. Based on (1), the arterial wall can be treated as a 1-DOF unit, as shown in Fig. 1(b)

$$m_{1} \cdot \frac{d^{2}x_{1}}{dt^{2}} + c_{1} \cdot \frac{dx_{1}}{dt} + k_{1} \cdot x_{1} = F_{1}(t)$$
with $F_{1}(t) = a\pi \Delta p(t)$ (2)

where m_1 , c_1 , and k_1 are mass, damping coefficient, and spring stiffness of the arterial wall, respectively,

$$m_1 = \rho \pi h a, \quad c_1 = -\frac{h}{a} \pi \eta, \quad k_1 = -\frac{h}{a} \pi E.$$
 (3)

For completeness, damping and inertial terms are included in (1) and (2), but in reality, the inertial term is negligible, as compared with the spring term [5]. Based on (2), when the damping term is negligible relative to the spring term, pulsatile pressure and arterial wall displacement have identical waveforms. When the damping term is not negligible, arterial wall displacement waveform is different from pulsatile pressure waveform [5].

As shown in Fig. 1(b), overlying tissue above the artery can be treated as another 1-DOF unit with its displacement $x_2(t)$ at the skin surface. Its spring stiffness, damping coefficient, and mass are denoted by k_2 , c_2 , and m_2 , respectively. The arterial wall and its overlying tissue form a 2-DOF model. Based on the force analysis of the 2-DOF model shown in Fig. 1(c), the governing equation of this 2-DOF model is given by the

following equation:

$$\begin{bmatrix} -\omega^{2}m + i\omega(c_{1} + c_{2}) + (k_{1} + k_{2}) & -i\omega c_{2} - k_{2} \\ -i\omega c_{2} - k_{2} & -\omega^{2}m_{2} + i\omega c_{2} + k_{2} \end{bmatrix} \times \begin{Bmatrix} x_{1} \\ x_{2} \end{Bmatrix} = \begin{Bmatrix} F_{1}(t) \\ 0 \end{Bmatrix}.$$
(4)

Based on (4), overlying tissue displacement and arterial wall displacement are related to driving force at the arterial wall by the following equation:

$$x_{2} = \frac{1}{\left[-\omega^{2}m_{1} + i\omega c_{1} + k_{1}\right]\left[\frac{-\omega^{2}m_{2}}{i\omega c_{2} + k_{2}} + 1\right] - \omega^{2}m_{2}}F_{1}$$
 (5a)
$$x_{1} = \frac{1}{\left[-\omega^{2}m_{1} + i\omega c_{1} + k_{1}\right] - \frac{(i\omega c_{2} + k_{2})\omega^{2}m_{2}}{i\omega c_{2} + k_{2} - \omega^{2}m_{2}}}F_{1}$$
 (5b)

$$x_{1} = \frac{1}{\left[-\omega^{2} m_{1} + i\omega c_{1} + k_{1}\right] - \frac{(i\omega c_{2} + k_{2})\omega^{2} m_{2}}{i\omega c_{2} + k_{2} - \omega^{2} m_{2}}} F_{1}$$
 (5b)

$$x_1 = \frac{-\omega^2 m_2 + i\omega c_2 + k_2}{i\omega c_2 + k_2} x_2.$$
 (5c)

Equation (5c) reveals the relation of arterial wall displacement to overlying tissue displacement. Evidently, when the inertial term of overlying tissue is negligible relative to the other two terms, arterial wall displacement and overlying tissue displacement are identical. In contrast, when the inertial term of the overlying tissue is non-negligible, the relation of pulsatile pressure and arterial wall displacement is affected by the overlying tissue, as shown in (5b).

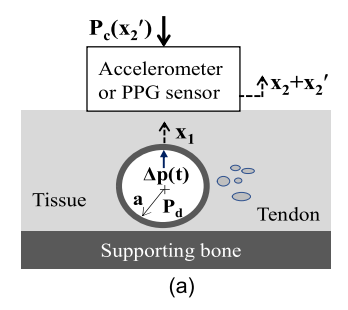
B. 2-DOF Model of the Artery-Sensor System With an Accelerometer and a PPG Sensor

An accelerometer needs to be fixed on a baseplate (or custom PCB) for arterial pulse measurement [6], [7]. Since the operation frequency bandwidth of an accelerometer is well above the first ten harmonics of an arterial pulse signal, it is reasonable to assume that the motion of an accelerometer is identical to that of its baseplate, so overlying tissue displacement is the accelerometer output. Consequently, the accelerometer is treated as sensor mass m_s , which is added to the overlying tissue. The combination of the overlying tissue, the accelerometer, and their contact interface, TCS unit, is treated as a 1-DOF unit, as shown in Fig. 2. While k_2 , c_2 , and m_2 of the TCS unit stem from the overlying tissue and contact interface, the mass of the TCS unit is the summation of m_2 and m_s . A PPG sensor employs optical transduction to measure arterial wall displacement [5]. Thus, a PPG sensor can also be treated as sensor mass m_s . The PPG sensor output is arterial wall displacement, instead of overlying tissue displacement. It should be noted that contact pressure P_c exerted on an accelerometer or a PPG sensor affects the values of k_2 , c_2 , and m_2 of the TCS unit.

According to Fig. 2(c), the governing equation of the 2-DOF model with an accelerometer or a PPG sensor becomes

$$\begin{bmatrix} -\omega^2 m_1 + i\omega(c_1 + c_2) + (k_1 + k_2) & -i\omega c_2 - k_2 \\ -i\omega c_2 - k_2 & -\omega^2 (m_2 + m_s) + i\omega c_2 + k_2 \end{bmatrix} \times \begin{bmatrix} x_1 \\ x_2 \end{bmatrix} = \begin{bmatrix} F_1(t) \\ 0 \end{bmatrix}.$$
 (6)

Then, the accelerometer output and the PPG sensor output are related to the driving force at the arterial wall by the following



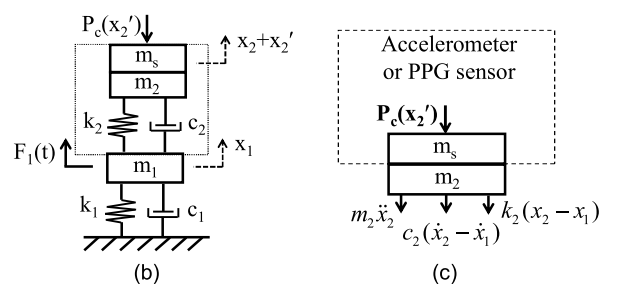


Fig. 2. Schematics of (a) artery-sensor system with a PPG sensor and an accelerometer, (b) its equivalent 2-DOF model with the dotted block representing the TCS unit, and (c) force analysis on mass $m_s + m_2$ of the TCS unit.

equation:

$$x_{2} = \frac{1}{\left[-\omega^{2} m_{1} + i\omega c_{1} + k_{1}\right] \left[1 + \frac{-r_{2}^{2}}{i2\zeta_{2}r_{2}+1}\right] - r_{2}^{2}k_{2}} F_{1} \text{ (Accele.)}$$
(7a)

$$x_{1} = \frac{1}{\left[-\omega^{2} m_{1} + i\omega c_{1} + k_{1}\right] - \frac{i2\zeta_{2}r_{2} + 1}{-r_{2}^{2} + i2\zeta_{2}r_{2} + 1}r_{2}^{2}k_{2}}F_{1} \text{ (PPG)}.$$
(7b)

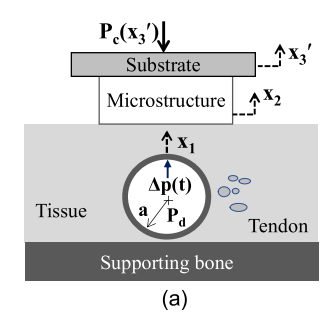
In (7), ω_2 and ζ_2 are the natural frequency and damping ratio of the TCS unit, respectively, and r_2 is the ratio of the frequency ω of the heart rate versus the natural frequency of the TCS

$$\omega_2 = \sqrt{\frac{k_2}{m_2 + m_s}}, \quad \zeta_2 = \frac{\omega_2 c_2}{2k_2}, \quad r_2 = \frac{\omega}{\omega_2}.$$
 (8)

The three parameters: k_2 , r_2 , and ζ_2 , of the TCS unit determine the difference between the true APW F_1 and the measured APW. According to (7), the measured APW always deviates from the true APW, as long as the inertial term of the TCS unit is non-negligible.

C. 2-DOF Model of the Artery-Sensor System With a Tactile Sensor

As shown in Fig. 3, a tactile sensor consists of a microstructure sitting on a substrate [8]. A force acting on its top deflects the microstructure, and this deflection is picked up by transducers underneath. Thus, the microstructure needs to be treated as a 1-DOF unit with its spring stiffness k_3 , damping coefficient c_3 , and mass m_s . Upon contact pressure P_c exerted on the substrate, the mass of the tactile sensor is added to the mass of the overlying tissue. The TCS unit still comprises of k_2 , c_2 , and $m_2 + m_s$. It is assumed that the



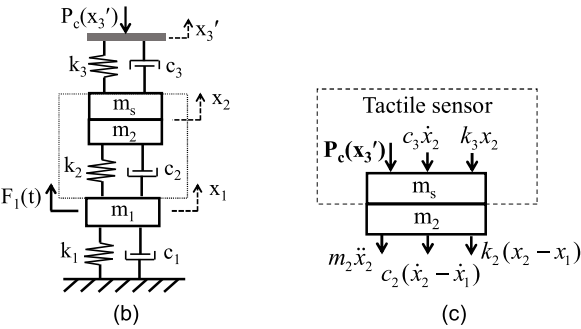


Fig. 3. Schematics of (a) artery-sensor system for a tactile sensor, (b) its equivalent 2-DOF model with the dotted block representing the TCS unit, and (c) force analysis on mass $m_{\rm S}+m_{\rm 2}$ of the TCS unit.

substrate is fixed. As compared to the 2-DOF model with an accelerometer and a PPG sensor, the 2-DOF model with a tactile sensor adds a spring k_3 and a damper c_3 to the other side of the TCS unit, without increasing the degree of freedom. According to Fig. 3(c), the governing equation of this 2-DOF model becomes (9), as shown at the bottom of the next page. The tactile sensor output and the arterial wall displacement are (10a) and (10b), as shown at the bottom of the next page, respectively, where ζ_3 is the damping ratio of the tactile sensor, and r_3 is the ratio of the frequency ω of the heart rate versus natural frequency ω_3 of the tactile sensor

$$\omega_3 = \sqrt{\frac{k_3}{m_2 + m_s}}, \quad \zeta_3 = \frac{\omega_3 c_3}{2k_3}, \quad r_3 = \frac{\omega}{\omega_3}.$$
 (11)

Based on (10a), a low k_3 and a low c_3 will increase the measured pulse amplitude and meanwhile reduce the influence of the tactile sensor on the deviation of the measured APW from the true APW.

D. Calculation of Sensor Output From Pulsatile Pressure at the RA

Pulsatile pressure $\Delta p(t)$ in the time domain at the radial artery (RA) of healthy 25-year-old virtual subjects in a database [16] is chosen for calculation. At the RA, arterial elasticity is E=916 kPa; the arterial radius is a=1.31 mm; arterial thickness is h=0.2 mm; the heart rate is 72.9 beats per minute (bpm). The value of arterial viscosity is assumed to 1/1000 of the value of arterial elasticity so that the damping term of the arterial wall is negligible relative to its spring term. Then, the difference between the measured APW and the true APW is solely caused by the TCS unit (and k_3 and c_3 when a tactile sensor is used).

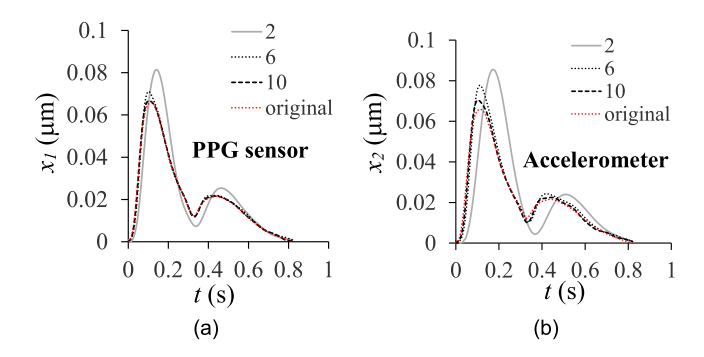


Fig. 4. Calculated APW from a PPG sensor and an accelerometer, with $k_2 = 1/4 \cdot k_1$, $\zeta_2 = 1$, and $r_2 = 2$, 6, 10: (a) output $x_1(t)$ of a PPG sensor and (b) output $x_2(t)$ of an accelerometer (note: original is the arterial wall displacement free of a sensor).

Despite being affected by overlying tissue, the measured APW still captures relatively conspicuous differences in the arterial wall itself [1], [2], [3], [5], [16], so k_2 should be smaller than k_1 . Here, it is assumed that $k_2 = 1/4 \cdot k_1$ and $1/6 \cdot k_1$. Given overlying tissue being soft tissue, the damping ratio of the TCS unit is assumed to be $\zeta_2 = 1$, 2 to examine its role in measured APW. The spring stiffness and damping ratio of the tactile sensor are assumed to be $k_3 = 1/10 \cdot k_2$ and $\zeta_3 = 1$.

The frequency ratio of the TCS unit is assumed to take three values: $r_2 = 2$, 6, 10. Pulsatile pressure $\Delta p(t)$ (the true APW) is a collection of harmonics of the heart rate and the first ten harmonics of the heart rate are commonly used to represent it. For healthy adults, lower harmonics (first and second) of $\Delta p(t)$ are dominant, relative to its higher harmonics (third-tenth) [5]. The natural frequency of the TCS unit determines which particular harmonic of $\Delta p(t)$ gets amplified, relative to the rest harmonics. The choice of the three values for r_2 is aimed to examine how amplifying lower and higher harmonics, respectively, of $\Delta p(t)$ affects the measured APW.

All the calculation is conducted in MATLAB. First, fast Fourier transform analysis (FFT) is conducted on $\Delta p(t)$ to obtain its first ten harmonics. Afterward, these ten harmonics are utilized to reconstruct $\Delta p(t)$ and calculate the driving force $F_1(t)$ in (2). Based on (7) and (10), $x_2(t)$ and $x_1(t)$ are calculated, and their first ten harmonics are also calculated through FFT analysis.

III. RESULTS

As shown in Fig. 4, the measured APW from both a PPG sensor and an accelerometer is significantly affected by the frequency ratio of the TCS unit. As shown in Fig. 5, the first ten harmonics of the measured APW deviate from their counterparts of the true APW. As shown in Figs. 6 and 7, although the damping ratio of the TCS unit also affects the measured APW, its role in measured APW is much less pronounced than the natural frequency of the TCS unit. Moreover, the influence of the damping ratio on measured APW varies with the frequency ratio of the TCS unit. As shown in Fig. 8, the influence of spring stiffness on measured APW is similar to that of damping ratio. The influence of spring stiffness on measured APW at $r_2 = 10$ is indiscernible and is not shown here. Taken together, when the natural frequency of the TCS unit stays away from the lower harmonics of the heart rate, the measured APW is less deviated from the true APW.

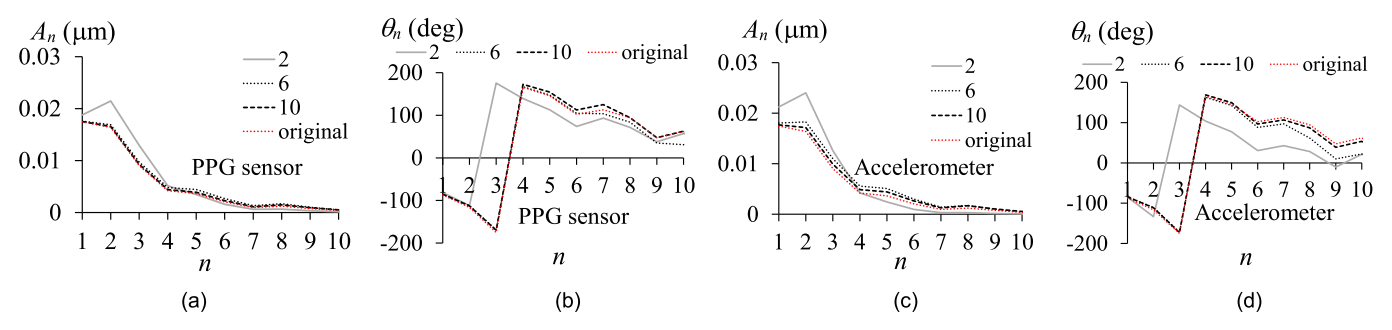


Fig. 5. First ten harmonics of the calculated APW from a PPG sensor and an accelerometer with $k_2 = 1/4$. k_1 and $\zeta_2 = 1$: (a) amplitudes, (b) phases of the output $x_1(t)$ of a PPG sensor, (c) amplitudes, and (d) phases of the output $x_2(t)$ of an accelerometer (note: original is the arterial wall displacement free of a sensor).

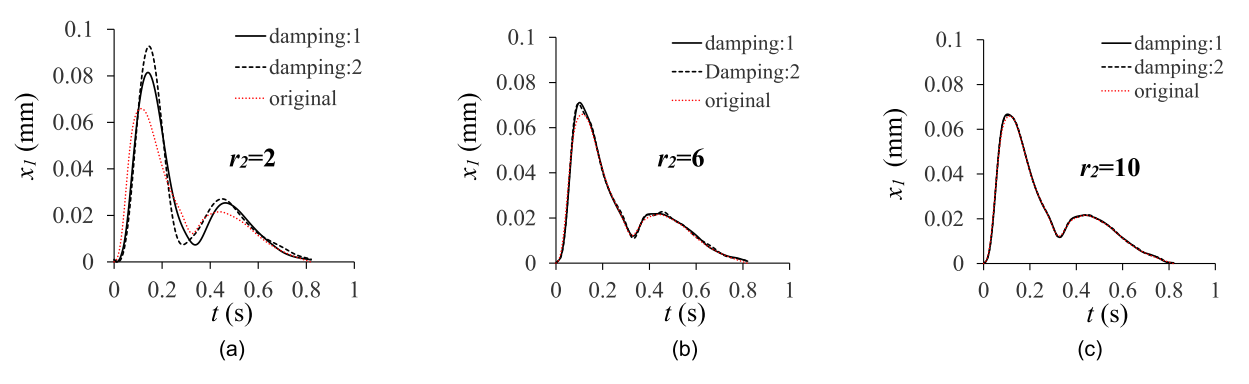


Fig. 6. Comparison of calculated APW from a PPG sensor between $\zeta_2 = 1$ and $\zeta_2 = 2$, with $k_2 = 1/4 \cdot k_1$: and $r_2 = 2$, 6, 10: (a) $r_2 = 2$, (b) $r_2 = 6$, and (c) $r_2 = 10$ (note: original is the arterial wall displacement free of a sensor).

Fig. 9 shows how the arterial wall displacement and the measured APW from a tactile sensor are affected by the frequency ratio of the TCS unit. The frequency ratio of the TCS unit greatly affects the measured APW from a tactile sensor. Similar to the measured APW of an accelerometer and a PPG sensor, the harmonics of the measured APW from a tactile sensor also deviate from their counterparts of the true APW and are not shown here. As shown in Fig. 10, the spring stiffness of the TCS unit affects the measured APW from a tactile sensor, when $r_2 = 2$ and 6. The influence of spring stiffness on the measured APW at $r_2 = 10$ is indiscernible and is not shown here.

To examine how the addition of k_3 and c_3 affects the measured APW, the measured APW from an accelerometer and a tactile sensor is plotted in Fig. 11. The addition of k_3 and c_3 affects the measured APW, and their influence on measured APW is still noticeable as frequency ratio of the TCS unit goes up.

Key features in the measured APW and its time-derivatives include the amplitude $x_{\rm max}$ of measured APW, the peak $v_{\rm max}$ of its first-order time derivative (or velocity), and maximum $a_{\rm max}$ and minimum $a_{\rm min}$ of its second-order time derivative (or acceleration) [1]. These key features of the calculated APW are summarized in Table I. Note that $|a_{\rm min}/a_{\rm max}|$ (or b/a) is commonly used as an index for arterial stiffness [1]. Evidently, the key features all deviate from their original (true) counterparts in the artery to some extent.

IV. DISCUSSION

A. Qualitative Validation of the 2-DOF Model With Related Experimental Findings in the Literature

While quite a few experimental studies focused on the influence of contact pressure on measured APW using a PPG sensor [3], [11], [12], [13], [14], Wang et al. [10] conducted an experimental study on the influence of contact pressure and sensor type on measured APW from the same group of

$$\begin{bmatrix} -\omega^{2}m_{1} + i\omega(c_{1} + c_{2}) + (k_{1} + k_{2}) & -i\omega c_{2} - k_{2} \\ -i\omega c_{2} - k_{2} & -\omega^{2}(m_{2} + m_{s}) + i\omega(c_{2} + c_{3}) + (k_{2} + k_{3}) \end{bmatrix} \begin{bmatrix} x_{1} \\ x_{2} \end{bmatrix} = \begin{bmatrix} F_{1} \\ 0 \end{bmatrix}$$
(9)
$$x_{2} = \frac{1}{\left(-\omega^{2}m_{1} + i\omega c_{1} + k_{1}\right) \left\{1 + \frac{-r_{2}^{2} + (i2\zeta_{3}r_{3} + 1)\frac{k_{3}}{k_{2}}}{i2\zeta_{2}r_{2} + 1}\right\} - r_{2}^{2}k_{2} + (i2\zeta_{3}r_{3} + 1)k_{3}} F_{1} \text{ (tactile sensor)}$$
(10a)
$$x_{1} = \frac{1}{\left(-\omega^{2}m_{1} + i\omega c_{1} + k_{1}\right) - \frac{(i2\zeta_{2}r_{2} + 1)\left[r_{2}^{2} - (i2\zeta_{3}r_{3} + 1)\frac{k_{3}}{k_{2}}\right]}{-r_{2}^{2} + i2\zeta_{2}r_{2} + 1 + (i2\zeta_{3}r_{3} + 1)\frac{k_{3}}{k_{2}}}} F_{1} \text{ (Arterial wall)}$$
(10b)

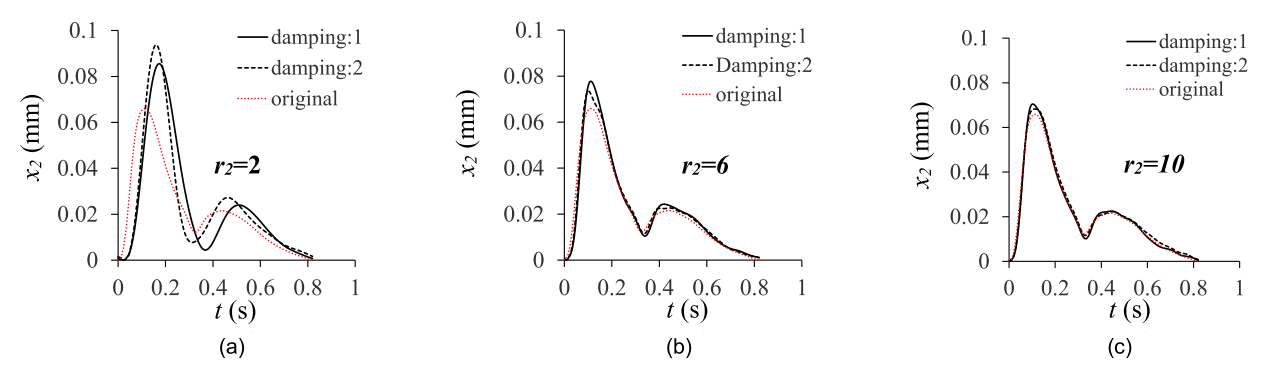


Fig. 7. Comparison of calculated APW from an accelerometer between $\zeta_2 = 1$ and $\zeta_2 = 2$, with $k_2 = 1/4$. k_1 : (a) $r_2 = 2$, (b) $r_2 = 6$, and (c) $r_2 = 10$ (note: original is the arterial wall displacement free of a sensor).

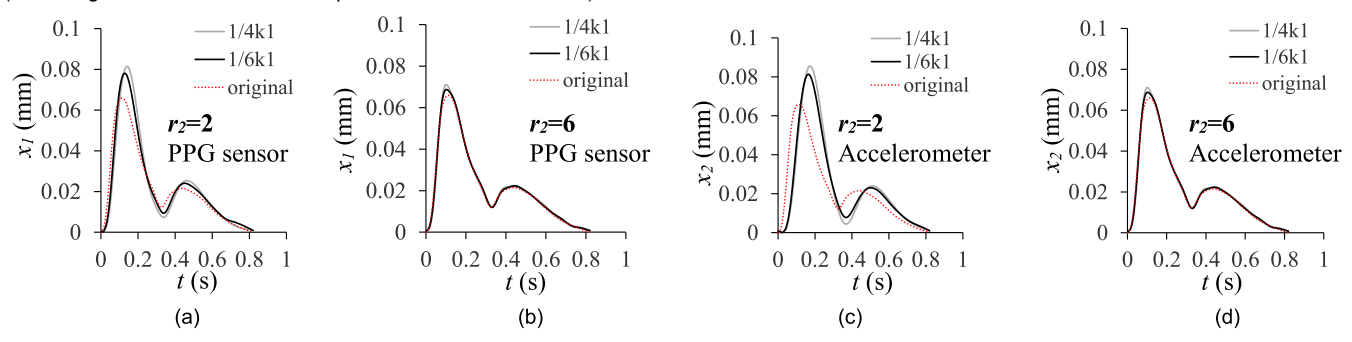


Fig. 8. Comparison of calculated APW between $k_2 = 1/4 \cdot k_1$ and $k_2 = 1/6 \cdot k_1$ with $\zeta_2 = 1$: (a) $r_2 = 2$, (b) $r_2 = 6$ from a PPG sensor, (c) $r_2 = 2$, and (d) $r_2 = 6$ from an accelerometer (note: original is the arterial wall displacement free of a sensor).

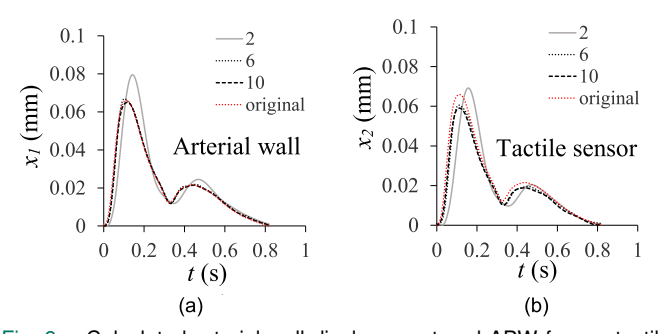


Fig. 9. Calculated arterial wall displacement and APW from a tactile sensor with $k_2=1/4$. k_1 , $\zeta_2=1$, and $r_2=2$, 6, 10, $k_3=1/10$. k_2 , and $\zeta_3=1$: (a) arterial wall displacement $x_1(t)$ and (b) output $x_2(t)$ of a tactile sensor (note: original is the arterial wall displacement free of a sensor).

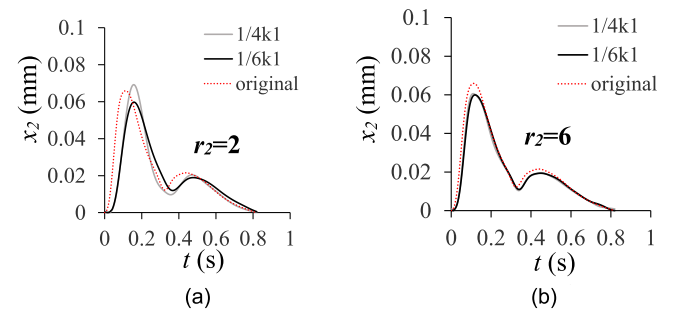


Fig. 10. Comparison of calculated APW between $k_2=1/4 \cdot k_1$ and $k_2=1/6 \cdot k_1$ from a tactile sensor with $\zeta_2=1$, $k_3=1/10 \cdot k_2$, and $\zeta_3=1$: (a) $r_2=2$ and (b) $r_2=6$ from a tactile sensor (note: original is the arterial wall displacement free of a sensor).

subjects. Here, the calculated results from the 2-DOF model are qualitatively compared with the experimental findings in these studies from three aspects: the influence of contact pressure on measured pulse amplitude, the influence of contact

pressure on measured APW, and the influence of sensor type on measured APW.

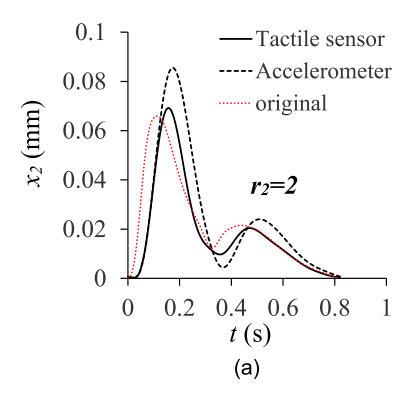
Regardless of the sensor type, the measured pulse amplitude was found to increase with contact pressure and reach maximum at medium pressure [10]. As shown in Figs. 4 and 8–10, the measured pulse amplitude increases with reduced natural frequency (or r_2) and increased spring stiffness k_2 of the TCS unit. As will be explained later on, increased contact pressure is associated with reduced natural frequency and increased spring stiffness of the TCS unit.

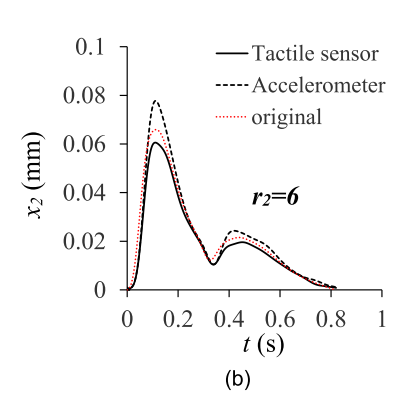
Regardless of the sensor type, changes in contact pressure cause changes in the dynamic parameters of the TCS unit, and then variations in measured APW. As shown in Figs. 4 and 8–10, and Table I, the foot, peak, and key features of the measured APW are all varied by changes in dynamic parameters of the TCS unit. This observation is consistent with the related experimental findings with PPG sensors [3], [11], [12], [13], [14] and accelerometers and tactile sensors [10].

As shown in Figs. 4 and 11, the measured APW varies between a PPG sensor, an accelerometer, and a tactile sensor, even with the same true APW and the same k_1 (or the same subject). This observation is consistent with the experimental finding that the measured APW from the same subject varies with the sensor type under medium pressure [10].

B. Dynamic Parameters (k_2 , c_2 , and ω_2) of the TCS Unit are a Collective Behavior of Contact Pressure, Overlying Tissue, and the Sensor

1) Contact Pressure: In the acoustical field, a vibratorground system has been extensively studied for the influence of





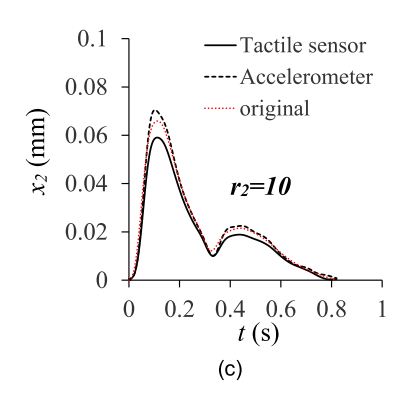


Fig. 11. Comparison of normalized APWs between an accelerometer and a tactile sensor with $k_2 = 1/4 \cdot k_1$, $\zeta_2 = 1$, and $k_3 = 1/10 \cdot k_2$, $\zeta_3 = 1$: (a) $r_2 = 2$, (b) $r_2 = 6$, and (c) $r_2 = 10$ (note: original is the arterial wall displacement free of a sensor).

contact pressure on the response of the ground, where contact pressure is found to increase k_2 and c_2 but decreases ω_2 [17]. The artery-sensor system in pulse measurement is analogous to a vibrator-ground system. Accordingly, the results from a vibrator-ground system are directly adopted to examine the influence of contact pressure on measured APW. In the following discussion, it is assumed that overlying tissue and the sensor remain the same.

Prior to contact pressure being applied, there is no microscopic-level contact between the overlying tissue and the sensor, k_2 , c_2 , and ω_2 of the TCS unit do not exist, so the sensor output is zero. Upon contact pressure, microscopic-level contact [17] is established between the overlying tissue and the sensor, and k_2 , c_2 , and ω_2 take limited values, allowing the pulse signal in the artery transmitted into the sensor.

At low contact pressure, k_2 and c_2 are small, but ω_2 is large. Thus, the denominator in (7) and (10a) is large, and the sensor captures a small pulse signal. As contact pressure increases to medium, k_2 and c_2 increase but ω_2 decreases. Thus, the denominator in (7) and (10a) becomes smaller, and the measured pulse signal becomes larger. At high contact pressure, pulsatile pressure is severely suppressed. A small denominator is not sufficient to compensate for suppression in pulsatile pressure and then the measured pulse signal becomes smaller. As shown in (10a), minimizing k_3 and c_3 of the tactile sensor will increase the measured pulse amplitude and reduce the deviation of the measured APW.

Increased measured pulse amplitude with contact pressure is achieved at the expense of increased deviation of measured APW from the true APW. As shown in (7) and (10a), the TCS unit serves as a harmonics-dependent transfer function from the true APW (pulsatile pressure) to the measured APW. As such, the measured APW always deviates from the true APW.

As shown in Figs. 4 and 9, the deviation of the measured APW from the true APW varies greatly with ω_2 of the TCS unit. It is known that harmonics of pulsatile pressure vary with CV conditions [5]. Overall, the lower harmonics of pulsatile pressure are dominant [5]. This explains why the measured APW with $r_2 = 2$ ($\omega_2 = 2\omega$) exhibits great deviation from the true APW. In contrast, higher harmonics of pulsatile pressure are not dominant, and thus the measured APW with $r_2 = 6$ or

10 does not show much deviation from the true APW. As such, ω_2 of the TCS unit needs to stay away from low harmonics of pulsatile pressure to minimize the deviation of the measured APW. Similarly, c_2 of the TCS unit should be minimized to alleviate its influence on the deviation of the measured APW.

Although low contact pressure provides a less-deviated measured APW, it leads to a small pulse signal embedded with large noise and thus a measured APW with significant noise-caused distortion. As such, it is a practical consideration to treat the measured APW with the maximum amplitude as the one best representing the true APW in an artery.

2) Overlying Tissue: Given the same sensor and under medium pressure (varying with overlying tissue), it was observed that thick overlying tissue in a high-BMI subject makes a measured pulse signal extremely small [1], [9], compared to a normal-BMI subject. Whereas thick overlying tissue offers a high k_2 , it provides a much lower ω_2 (i.e., a much higher m_2). Based on (7) and (10a), the role of k_2 of the TCS unit is embedded in ω_2 . This explains the difficulty in measuring a clear pulse signal from a high-BMI subject and the need to calibrate the measured pulse amplitude with blood pressure at the brachial artery [9]. Note that the influence of overlying tissue on measured APW discussed here is rather simplified, since the anatomical complexity of overlying tissue may further complicate its influence on measured APW.

3) Sensor: Based on (7) and (10a), only the mass m_s of the sensor is explicitly included in the TCS unit. Yet, as shown in Figs. 2 and 3 and explained in Section II, m_2 , c_2 and ω_2 of the TCS unit are affected by how the sensor conforms to overlying tissue under contact pressure because such conformity determines the microscopic-level contact between overlying tissue and the sensor. As such, the sensor also plays a role in affecting m_2 , c_2 , and ω_2 of the TCS unit. Yet, due to the anatomical complexity of overlying tissue, it is difficult to explicitly evaluate the influence of a sensor on m_2 , c_2 , and ω_2 of the TCS unit.

Currently, one of the main concerns in pulse measurement is that a measured pulse signal is small and suffers from large noise. Different sensor designs have been tried to improve the conformity of a sensor to overlying tissue to maximize the measured pulse amplitude [9]. Certainly, different sensor designs alter the values of m_2 , c_2 , and ω_2 , given the same

TABLE I
CALCULATED VALUES OF THE KEY FEATURES OF THE CALCULATED APW AND ITS TWO TIME DERIVATIVES FROM THE THREE TYPES OF SENSOR
(NOTE THAT: $k_1 = 4.32 \times 10^3$ N/m, $c_1 = 432$ N·s/m, $m_1 = 0.8 \times 10^{-3}$ kg, and $\omega = 2\pi \cdot 1.22$ Hz)

		x_{max} (mm)	$v_{max} (\text{mm/s}^2)$	$a_{max} (\text{mm/s}^2)$	a_{min} (mm/s ²)	$a_{min}/a_{max} = b/a$
Free of sensor	True	0.066	1.19	34.50	-30.77	0.89
PPG sensor $\zeta_2=1$, $k_2=1/4k_1$	$r_2 = 2$	0.081	1.12	25.52	-20.91	0.82
	$r_2 = 6$	0.071	1.38	38.27	-44.08	1.15
	$r_2 = 10$	0.066	1.30	38.69	-38.70	1.00
Accelerometer $\zeta_2=1$, $k_2=1/4k_1$	$r_2 = 2$	0.085	1.00	19.10	-19.21	1.01
	$r_2 = 6$	0.077	1.45	38.57	-45.03	1.17
	$r_2 = 10$	0.070	1.40	40.30	-44.56	1.11
PPG sensor $\zeta_2=2$, $k_2=1/4k_1$	$r_2 = 2$	0.093	1.24	24.98	-29.64	1.19
	$r_2 = 6$	0.070	1.47	42.73	-52.87	1.24
	$r_2 = 10$	0.066	1.31	39.15	-39.59	1.01
Accelerometer $\zeta_2=2$, $k_2=1/4k_1$	$r_2 = 2$	0.093	1.21	22.57	-28.79	1.28
	$r_2 = 6$	0.073	1.50	43.20	-53.51	1.24
	$r_2 = 10$	0.068	1.35	40.37	-40.76	1.01
Tactile sensor $\zeta_2=2$, $k_2=1/4k_1$ $\zeta_3=1$, $k_3=1/10k_2$	$r_2 = 2$	0.069	0.90	17.99	-20.31	1.13
	$r_2 = 6$	0.060	1.17	33.38	-35.55	1.07
	$r_2 = 10$	0.059	1.11	32.15	-31.32	0.97

subject and under the same contact pressure. Another main concern is that alignment variations of the sensor between measurements also alter the values of m_2 , c_2 , and ω_2 of the TCS unit, as evidenced by commonly recorded standard deviations of different measurements in experimental studies [2], [9], [18].

4) Entangled Influence of Contact Pressure, Overlying Tissue, and the Sensor on Measured APW: Although the role of k_2 , c_2 , and ω_2 of the TCS unit in measured APW is clarified in (7) and (10a), it should be emphasized that their values are collectively determined by contact pressure, overlying tissue, and the sensor, as discussed above. Only when the other two factors are fixed, can the influence of each factor on measured APW become clear.

With the true APW and the measured APW as the input and the output, respectively, it is insufficient to get an accurate estimate of the values of k_2 , c_2 , and ω_2 . Their values are not expected to vary linearly with contact pressure, due to the anatomical complexity of overlying tissue. Thus, the variation of measured APW with contact pressure has limited capability for accurately estimating their values. As such, an accurate quantitative validation of the 2-DOF model is out of reach. Yet, to alleviate the influence of the TCS unit on measured APW, an approximate estimate of the values of k_2 , c_2 , and ω_2 might be obtained by adjusting their values until the measured APW is maximally matched to the true APW [19].

Given all the above-mentioned concerns (i.e., noise, alignment variations, and motion artifacts, as will be discussed later on), arterial pulse measurement encompasses more complexity, in addition to the three factors. Nonetheless, the 2-DOF model of the artery-sensor system clarifies the role of contact pressure, overlying tissue, and the sensor in measured APW and reveals the importance of considering these factors in the interpretation of measured APW for clinical values.

C. Myth of Transmural Pressure

It is well established that as contact pressure increases, measured arterial elasticity decreases [11]. This experimental finding has been explained by the influence of transmural

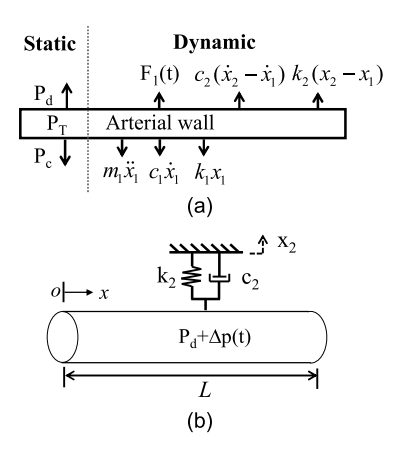


Fig. 12. Influence of a sensor on the artery in pulse measurement. (a) Negative dynamic forces exert on the arterial wall and (b) k_2 and c_2 alter pulse wave propagation in the arterial segment.

pressure on arterial elasticity. As the pressure in the circumferential direction of the arterial wall, transmural pressure P_T is the difference between diastolic blood pressure P_d and external pressure outside the artery. Transmural pressure sets the value of arterial elasticity. Since contact pressure P_c is an indicator of external pressure outside the artery, transmural pressure is set by contact pressure: $P_T \propto P_d - P_c$. As contact pressure increases, transmural pressure goes down and then arterial elasticity is reduced.

As shown in Fig. 12(a), in a pulse measurement, while contact pressure as a static force is applied to the arterial wall, dynamic forces are also exerted on the arterial wall. Accordingly, (2) the dynamic behavior of the arterial wall needs to be expanded to include negative dynamic forces from the TCS unit

$$m_{1} \cdot \frac{d^{2}x_{1}}{dt^{2}} + c_{1} \cdot \frac{dx_{1}}{dt} + k_{1} \cdot x_{1}$$

$$-\left\{k_{2}(x_{2} - x_{1}) + c_{2} \cdot \left(\frac{dx_{2}}{dt} - \frac{dx_{1}}{dt}\right)\right\}$$

$$= a\pi \Delta p(t). \tag{12}$$

Based on (7), measured APW from a PPG sensor is related to $\Delta p(t)$ in an artery by (13), as shown at the bottom of the page. Similarly, measured APW from an accelerometer is related to $\Delta p(t)$ in an artery by (14), as shown at the bottom of the page. Based on (10a), measured APW from a tactile sensor is related to $\Delta p(t)$ in an artery by (15), as shown at the bottom of the page. With a tactile sensor, arterial wall displacement is related to $\Delta p(t)$ in an artery by (16), as shown at the bottom of the page. Although transmural pressure may affect arterial elasticity (or k_1), dynamic forces from the TCS unit contribute negatively to the spring stiffness of the arterial wall, and thus the measured arterial elasticity is reduced by lower transmural pressure.

D. Motion Artifacts are Not Merely Baseline Drift

Motion artifacts, namely respiration, body motion, and nonideal fixing of a sensor at the artery, are all low-frequency noise and cause distortion in the measured APW [1], [2], [3]. Currently, motion artifacts are commonly removed from the measured pulse signal by using a low pass filter, and baseline drift obtained from motion artifacts removal is commonly considered as motion artifacts. Here, motion artifacts are added to the 2-DOF model for a theoretical analysis of its influence on measured APW

As shown in Fig. 2, motion artifacts cause displacement $x'_2(t)$ at the mass of the TCS unit, and this displacement further leads to time-dependent variation of dynamic parameters: $k_2 + k'_2(t)$, $c_2 + c'_2(t)$, and $m_2 + m'_2(t)$, of the TCS unit.

Consequently, the measured APW from a PPG sensor becomes (17), as shown at the bottom of the page. Similarly, the measured APW from an accelerometer becomes (18a), as shown at the bottom of the page. It should be noted that the original output from an accelerometer is the second-order time derivative of the measured APW, (18b), as shown at the bottom of the page. As shown in Fig. 3, the substrate of a tactile sensor is not firmly fixed. Motion artifacts cause displacement $x_3'(t)$ at the substrate. Then, the measured APW from a tactile sensor becomes (19), as shown at the bottom of the page.

To date, PPG sensors and tactile sensors are the two mostwidely used sensor types for arterial pulse measurement. Despite its low cost and small footprint, accelerometers have not been extensively used in pulse measurement. As shown in (18b), the original output of an accelerometer is an acceleration signal. As compared to PPG sensors and tactile sensors, the influence of motion artifacts on the accelerometer output is amplified by ω_2 time, which might explain the difficulty in extracting an accurately measured APW from the original acceleration signal [7].

As revealed in (17)–(19), due to the influence of contact pressure on dynamic parameters of the TCS unit, motion artifacts add multiplicative noise: $k'_2(t)$, $c'_2(t)$, and $m'_2(t)$, to the measured APW, in addition to additive noise (or baseline drift): $x'_2(t)$ and $x'_3(t)$. While additive noise can be easily removed by a low pass filter, multiplicative noise is extremely difficult to remove from the measured APW. This explains the

$$m_{1} \cdot \frac{d^{2}x_{1}}{dt^{2}} + \left(c_{1} - \frac{r_{2}^{2}}{-r_{2}^{2} + i2\zeta_{2}r_{2} + 1}c_{2}\right) \cdot \frac{dx_{1}}{dt} + \left(k_{1} - \frac{r_{2}^{2}}{-r_{2}^{2} + i2\zeta_{2}r_{2} + 1}k_{2}\right) \cdot x_{1} = a\pi \Delta p(t) \tag{13}$$

$$\left(1 + \frac{-r_{2}^{2}}{i2\zeta_{2}r_{2} + 1}\right)m_{1} \cdot \frac{d^{2}x_{2}}{dt^{2}} + \left(1 + \frac{-r_{2}^{2}}{i2\zeta_{2}r_{2} + 1}\right)c_{1}\frac{dx_{2}}{dt} + \left\{\left(1 + \frac{-r_{2}^{2}}{i2\zeta_{2}r_{2} + 1}\right)k_{1} - r_{2}^{2}k_{2}\right\}x_{2} = a\pi \Delta p(t) \tag{14}$$

$$\left(1 + \frac{-r_{2}^{2} + (i2\zeta_{3}r_{3} + 1)\frac{k_{3}}{k_{2}}}{i2\zeta_{2}r_{2} + 1}\right)m_{1} \cdot \frac{d^{2}x_{2}}{dt^{2}} + \left(1 + \frac{-r_{2}^{2} + (i2\zeta_{3}r_{3} + 1)\frac{k_{3}}{k_{2}}}{i2\zeta_{2}r_{2} + 1}\right)c_{1} \cdot \frac{dx_{2}}{dt} + \left\{\left(1 + \frac{-r_{2}^{2} + (i2\zeta_{3}r_{3} + 1)\frac{k_{3}}{k_{2}}}{i2\zeta_{2}r_{2} + 1}\right)c_{1} \cdot \frac{dx_{2}}{dt} + \left\{\left(1 + \frac{-r_{2}^{2} + (i2\zeta_{3}r_{3} + 1)\frac{k_{3}}{k_{2}}}{i2\zeta_{2}r_{2} + 1}\right)c_{1} \cdot \frac{dx_{2}}{dt} + \left\{\left(1 + \frac{-r_{2}^{2} + (i2\zeta_{3}r_{3} + 1)\frac{k_{3}}{k_{2}}}{i2\zeta_{2}r_{2} + 1}\right)c_{1} \cdot \frac{dx_{2}}{dt} + \left\{\left(1 + \frac{-r_{2}^{2} + (i2\zeta_{3}r_{3} + 1)\frac{k_{3}}{k_{2}}}{i2\zeta_{2}r_{2} + 1}\right)c_{1} \cdot \frac{dx_{2}}{dt} + \left\{\left(1 + \frac{-r_{2}^{2} + (i2\zeta_{3}r_{3} + 1)\frac{k_{3}}{k_{2}}}{i2\zeta_{2}r_{2} + 1}\right)c_{1} \cdot \frac{dx_{2}}{dt} + \left\{\left(1 + \frac{-r_{2}^{2} + (i2\zeta_{3}r_{3} + 1)\frac{k_{3}}{k_{2}}}{i2\zeta_{2}r_{2} + 1}\right)c_{1} \cdot \frac{dx_{2}}{dt} + \left\{\left(1 + \frac{-r_{2}^{2} + (i2\zeta_{3}r_{3} + 1)\frac{k_{3}}{k_{2}}}{i2\zeta_{2}r_{2} + 1}\right)c_{1} \cdot \frac{dx_{2}}{dt} + \left\{\left(1 + \frac{-r_{2}^{2} + (i2\zeta_{3}r_{3} + 1)\frac{k_{3}}{k_{2}}}{i2\zeta_{2}r_{2} + 1}\right)c_{1} \cdot \frac{dx_{2}}{dt} + \left\{\left(1 + \frac{-r_{2}^{2} + (i2\zeta_{3}r_{3} + 1)\frac{k_{3}}{k_{2}}}{i2\zeta_{2}r_{2} + 1}\right)c_{1} \cdot \frac{dx_{2}}{dt} + \left\{\left(1 + \frac{-r_{2}^{2} + (i2\zeta_{3}r_{3} + 1)\frac{k_{3}}{k_{2}}}{i2\zeta_{2}r_{2} + 1}\right)c_{1} \cdot \frac{dx_{2}}{dt} + \left\{\left(1 + \frac{-r_{2}^{2} + (i2\zeta_{3}r_{3} + 1)\frac{k_{3}}{k_{2}}}{i2\zeta_{2}r_{2} + 1}\right)c_{1} \cdot \frac{dx_{2}}{dt} + \left\{\left(1 + \frac{-r_{2}^{2} + (i2\zeta_{3}r_{3} + 1)\frac{k_{3}}{k_{2}}}{i2\zeta_{2}r_{2} + 1}\right)c_{1} \cdot \frac{dx_{2}}{dt} + \left\{\left(1 + \frac{-r_{2}^{2} + (i2\zeta_{3}r_{3} + 1)\frac{k_{3}}{k_{2}}}{i2\zeta_{2}r_{2} + 1}\right)c_{1} \cdot \frac{dx_{2}}{dt} + \left\{\left(1 + \frac{-r_{2}^{2} + (i2\zeta_{3}r_{3} + 1)\frac{k_{3}}{k_{2}}}{i2\zeta_{2}r_{2} + 1}\right)c_{1} \cdot \frac{dx_{2}}{dt} + \left\{$$

reason why various noise-filtering techniques [20] have been pursued for removing motion artifacts from measured APW, besides low-pass filtering. Given the difficulty in removing multiplicative noise [21] from measured APW, minimizing motion artifacts in pulse measurement is crucial for improving accuracy in measured APW.

E. Implications for Clinical Applications and Study Limitations

Besides the TCS unit, the artery and the true APW are also involved in pulse measurement. Here, with measured APW from an accelerometer chosen for illustration, the influence of individual variations on measured APW is examined. Based on (2), (3), and (7a), pertaining to arterial pulse measurement, individual variations include arterial parameters (h, a, and E), harmonics (amplitude Δp_n and phase φ_n of the nth harmonic and frequency ω of the heart rate) of the true APW, as well as overlying tissue and P_d . Note that overlying tissue and P_d are included in the dynamic parameters of the TCS unit. Equation (7a) can be rewritten as follows:

$$x_{2} = \frac{a\pi \sum_{n=1}^{10} \Delta p_{n} \cos(n\omega t + \phi_{n})}{\left(\frac{h}{a}\pi E\right) \left(1 - \frac{1}{i2\zeta_{2}\frac{n\omega}{\omega_{2}} + 1} \left(\frac{n\omega}{\omega_{2}}\right)^{2}\right) - \left(\frac{n\omega}{\omega_{2}}\right)^{2} k_{2}}$$
(Accele.).

For clarity, the inertial and damping terms of the arterial wall are omitted in (20). Thus, given the same dynamic parameters of the TCS unit, deviation of measured APW from the true APW varies with individuals, since arterial parameters and harmonics of the true APW vary with individuals. This indicates that the deviation of measured APW from the true APW varies with CV conditions (e.g., young versus old), given the same dynamic parameters of the TCS unit. It is worth noting that individual variations among healthy subjects of the same characteristics should be minuscule.

As discussed above, the existence of the TCS unit in pulse measurement causes deviation of measured APW from the true APW and such deviation varies with individuals, given the same dynamic parameters of the TCS unit. Yet, since numerous clinical studies have identified the capability of measured APW distinguishing relatively conspicuous differences between healthy and a nonhealthy condition [1], [5], deviation of measured APW caused by the TCS unit and other factors (e.g., the true APW being affected and the TCS unit exhibiting nonlinear behavior) should be relatively moderate.

There are two major study limitations. One is the assumption of true APW being unchanged by the TCS unit. As shown in Fig. 12(b), the addition of the TCS unit somewhere in the arterial segment is equivalent to modifying local arterial viscoelasticity at the measurement site, which will alter pulse wave propagation in the arterial segment. Thus, true APW at the measurement site is affected by the TCS unit. As shown in (13) and (16), as far as the dynamic forces from the TCS unit are relatively small, as compared with its counterparts of the arterial wall, this alternation is insignificant and then this assumption is relatively realistic. The other limitation is the assumption of the constant values of dynamic parameters of the TCS unit in a pulse cycle. This indicates the linear behavior

of overlying tissue and tissue-sensor contact interface. It might be likely that the TCS unit behaves nonlinearly in a pulse cycle, causing further deviation of the measured APW from the true APW.

In the future, the finite element model of the artery-sensor system could be employed to evaluate the extent to which the TCS unit affects the true APW, examine how the nonlinear behavior of the TCS unit affects measured APW, as well as study the influence of arterial parameters and harmonics of the true APW on the deviation of measured APW from the true APW. System identification techniques may be explored to analyze the variation of the measured APW with contact pressure for an approximate estimation of the values of dynamic parameters of the TCS unit so that the influence of the TCS unit on measured APW might be alleviated to allow detecting a relatively fine difference in true APW.

V. CONCLUSION

In this study, a 2-DOF model of the artery-sensor system is developed that accounts for contact pressure, sensor type, and overlying tissue for interpreting variability in measured APW. The developed theory and the accompanying calculation allow a qualitative explanation of the related experimental findings in the literature. The key conclusions from this study are as follows.

- Formed by overlying tissue, sensor, and their contact interface, the TCS unit as a 1-DOF unit serves as a harmonics-dependent transfer function from the true APW (pulsatile pressure in the artery) to the measured APW. As such, the measured APW always deviates from the true APW.
- Experimentally observed influence of contact pressure on measured APW is identified as the influence of contact pressure on dynamic parameters of the TCS unit.
- The influence of transmural pressure on arterial elasticity stems from negative dynamic forces on the arterial wall exerted by the TCS unit.
- 4) Motion artifacts introduce not merely baseline drift, but also multiplicative noise to the measured APW, due to their influence on the dynamic parameters of the TCS unit.
- 5) Interpretation of the measured APW for clinical values must consider the influence of contact pressure, sensor used, and overlying tissue when a relatively fine difference [18] in true APW needs to be detected.

This work is the first attempt to provide a dynamic model that allows relating the three key factors identified in experimental studies to measured APW. The finding on the role of motion artifacts on measured APW underscores the importance of minimizing motion artifacts for improving accuracy in measured APW. Given the great complexity of arterial pulse measurement, a tremendous amount of work needs to be conducted for a quantitative study of measured APW with the 2-DOF model in the future.

REFERENCES

 M. Elgendi, "On the analysis of fingertip photoplethysmogram signals," *Current Cardiol. Rev.*, vol. 8, no. 1, pp. 14–25, Jun. 2012, doi: 10.2174/157340312801215782.

- [2] D. Wang, L. Reynolds, T. Alberts, L. Vahala, and Z. Hao, "Model-based analysis of arterial pulse signals for tracking changes in arterial wall parameters: A pilot study," *Biomech. Model. Mechanobiol.*, vol. 18, no. 6, pp. 1629–1638, May 2019, doi: 10.1007/s10237-019-01165-x.
- [3] A. Chandrasekhar, M. Yavarimanesh, K. Natarajan, J.-O. Hahn, and R. Mukkamala, "PPG sensor contact pressure should be taken into account for cuff-less blood pressure measurement," *IEEE Trans. Biomed. Eng.*, vol. 67, no. 11, pp. 3134–3140, Nov. 2020, doi: 10.1109/TBME.2020.2976989.
- [4] X. Ding, B. P. Yan, Y.-T. Zhang, J. Liu, N. Zhao, and H. K. Tsang, "Pulse transit time based continuous cuffless blood pressure estimation: A new extension and a comprehensive evaluation," *Sci. Rep.*, vol. 7, no. 1, p. 11554, Sep. 2017, doi: 10.1038/s41598-017-11507-3.
- [5] Z. Hao, "Relations of radial vibration of the arterial wall to pulsatile parameters in blood flow for extraction of arterial indices," *J. Eng. Sci. Med. Diag. Therapy*, vol. 6, no. 1, Feb. 2023, Art. no. 011002, doi: 10.1115/1.4055390.
- [6] N. Di Lascio et al., "Noninvasive assessment of carotid pulse pressure values: An accelerometric-based approach," *IEEE Trans. Biomed. Eng.*, vol. 63, no. 4, pp. 869–875, Apr. 2016, doi: 10.1109/TBME.2015.2477538.
- [7] R. Arathy, P. M. Nabeel, V. V. Abhidev, M. Sivaprakasam, and J. Joseph, "An accelerometric sensor system with integrated hydrostatic pressure correction to assess carotid arterial stiffness," *IEEE Sensors J.*, vol. 21, no. 9, pp. 11163–11175, May 2021, doi: 10.1109/JSEN.2021.3059292.
- [8] D. Wang, J. Shen, L. Mei, S. Qian, J. Li, and Z. Hao, "Performance investigation of a wearable distributed-deflection sensor in arterial pulse waveform measurement," *IEEE Sensors J.*, vol. 17, no. 13, pp. 3994–4004, Jul. 2017, doi: 10.1109/JSEN.2017.2704903.
- [9] Z. Hao and D. Wang, "Arterial pulse signal amplification by adding a uniform PDMS layer to a pyrex-based microfluidic tactile sensor," *IEEE Sensors J.*, vol. 20, no. 4, pp. 2164–2172, Feb. 2020, doi: 10.1109/JSEN.2019.2949503.
- [10] H. Wang et al., "Quantitative comparison of the performance of piezoresistive, piezoelectric, acceleration, and optical pulse wave sensors," *Front Physiol.*, vol. 10, p. 1563, Jan. 2020, doi: 10.3389/fphys.2019.01563.
- [11] X.-F. Teng and Y.-T. Zhang, "Theoretical study on the effect of sensor contact force on pulse transit time," *IEEE Trans. Biomed. Eng.*, vol. 54, no. 8, pp. 1490–1498, Aug. 2007, doi: 10.1109/TBME.2007.900815.
- [12] F. S. Solberg, S. Kohtala, H. Vestad, and M. Steiner, "A combined photoplethysmography and force sensor prototype for improved pulse waveform analysis," in *Proc. IEEE Sensors*, Montreal, QC, Canada, Oct. 2019, pp. 1–4, doi: 10.1109/SENSORS43011.2019.8956487.
- [13] A. Grabovskis, Z. Marcinkevics, U. Rubins, and E. Kviesis-Kipge, "Effect of probe contact pressure on the photoplethysmographic assessment of conduit artery stiffness," *J. Biomed. Opt.*, vol. 18, no. 2, Feb. 2013, Art. no. 027004, doi: 10.1117/1.JBO.18.2.027004.

- [14] I. Pi, I. Pi, and W. Wu, "External factors that affect the photoplethys-mography waveforms," *Social Netw. Appl. Sci.*, vol. 4, no. 1, p. 21, Jan. 2022, doi: 10.1007/s42452-021-04906-9.
- [15] R. C. B. Roxas et al., "A theoretical study of sensor-artery interaction in noninvasive arterial pulse signal measurement using tactile sensors," in *Proc. ASME Int. Mech. Eng. Congr. Expo.*, vol. 5, Nov. 2020, Paper no. V005T05A037, doi: 10.1115/IMECE2020-24570.
- [16] P. H. Charlton, J. M. Harana, S. Vennin, Y. Li, P. Chowienczyk, and J. Alastruey, "Modeling arterial pulse waves in healthy aging: A database for in silico evaluation of hemodynamics and pulse wave indexes," *Amer. J. Physiol.-Heart Circulatory Physiol.*, vol. 317, no. 5, pp. H1062–H1085, Nov. 2019.
- [17] R. Noorlandt and G. Drijkoningen, "On the mechanical vibrator-earth contact geometry and its dynamics," *Geophysics*, vol. 81, no. 3, pp. 23–31, May 2016, doi: https://doi.org/10.1190/geo2015-0271.1.
- [18] H. Tanaka, "Various indices of arterial stiffness: Are they closely related or distinctly different?" *Pulse*, vol. 5, nos. 1–4, pp. 1–6, Mar. 2018, doi: 10.1159/000461594.
- [19] K. S. Matthys et al., "Pulse wave propagation in a model human arterial network: Assessment of 1-D numerical simulations against in vitro measurements," *J. Biomech.*, vol. 40, no. 15, pp. 3476–3486, 2007, doi: 10.1016/j.jbiomech.2007.05.027.
- [20] D. Pollreisz and N. TaheriNejad, "Detection and removal of motion artifacts in PPG signals," *Mobile Netw. Appl.*, vol. 27, no. 2, pp. 728–738, Apr. 2022.
- [21] C. Li and C. He, "Fractional-order diffusion coupled with integer-order diffusion for multiplicative noise removal," *Comput. Math. Appl.*, vol. 136, pp. 34–43, Apr. 2023, doi: 10.1016/j.camwa.2023.01.036.

Zhili Hao received the Ph.D. degree in mechanical engineering from the University of Central Florida, Orlando, FL, USA, in 2000.

She worked in telecommunications industry for two years before she came back to academia and did postdoctoral research in electrical engineering. Since 2006, she has been a Faculty Member with the Department of Mechanical and Aerospace Engineering, Old Dominion University, Norfolk, VA, USA. Her past research focused on development of various micro-sensors, including gyroscopes, resonators, and microfluidic-based tactile sensors and investigation of mechanics crucial for performance improvement of micro-sensors. Her current research interests include experimental studies and theoretical studies of arterial pulse signal for cardiovascular disease detection and cardiovascular physiology.